Hindawi
Geofluids
Volume 2019, Article ID 1309042, 9 pages
https://doi.org/10.1155/2019/1309042

Research Article

A Method of Differentiating the Early-Time and Late-Time Behavior in Pressure-Pulse Decay Permeametry

Yu Zhao,[1] **Chaolin Wang**,[1] **Yongfa Zhang**,[2] **and Qiang Liu**[2]

[1]*School of Civil Engineering, Guizhou University, Guiyang 550025, Guizhou, China*
[2]*School of Civil Engineering, Chongqing University, Chongqing 400045, China*

Correspondence should be addressed to Chaolin Wang; 20151601005@cqu.edu.cn

Received 22 October 2018; Accepted 18 February 2019; Published 9 April 2019

Academic Editor: Craig T. Simmons

The pressure-pulse decay is a preferred technique for determining permeability of unconventional gas reservoir rocks. The pressure-pulse decay often shows quite different characteristics during the early time and the later time. Most approaches for estimating the permeability proposed in the literature are required to use the later-time pressure-pulse decay measurements. However, the later-time data are often selected subjectively, lacking a universal criterion. In this paper, a method of differentiating the early-time and late-time behavior for pressure-pulse decay test is proposed. The analytical results show that the critical time (dimensionless time) of early-/late-time decay characteristics mainly depends on the volume ratios, and it increases first and then decreases with the volume ratios. The critical time for cases with same chamber sizes is much less than that for cases with unequal chamber sizes. Applicability of the proposed methods is examined using a numerical simulator, TOUGH+REALGASBRINE. The numerical results show that the pressure gradient along the sample varies nonlinearly at the early time and becomes a constant at the late time. Then, the proposed method is applied to real data for permeability estimation. It is found that the early-time behavior is negligible as the volume ratio takes on small values. As the volume ratios increase, the deviation becomes significant and considerable permeability errors will be produced if these early-time data are used.

1. Introduction

Permeability is typically considered the critical parameter for commercial gas production [1–3], geological storage facilities for CO_2 [4], and radioactive waste storage [5]. Quantitative description and modeling of single-phase flow or multiphase flow in porous media require accurate estimation of permeability and the relationship between capillary pressure, saturation, and permeability [6–8]. The pressure-pulse decay is a widely used method for permeability measurement of tight rocks. It is initially proposed by Brace et al. [9] for the determination of permeability in tight rocks. This technique is based on the analysis of the differential pressure between the upstream and downstream circuits within a sample. Note that Brace's solution assumed constant pressure gradient in the sample and ignored compressive storage effect. Hsieh et al. [10] and Dicker and Smits [11] extended Brace's model to include compressive storage effect in their analytical solutions of the problem. Jones [12] introduced a factor "f" to simplify Dicker and Smits's solution, which was further developed by Cui et al. [13] by taking consideration of sorption effects. Moreover, multiple optimized methodologies have been developed based on the conventional pulse decay technique. Lasseux et al. [14] suggested a step decay method that enables accurate, simultaneous characterization of the Klinkenberg-corrected permeability, Klinkenberg coefficient, and porosity from gas permeability experiments. Yang et al. [15] presented a modified pressure-pulse decay method for determining permeabilities of tight reservoir cores. In their method, only one gas chamber is applied at one end of the test core sample, while the other end of the core is sealed. Feng et al. [16] proposed a new experimental design by creating dual pressure pulses to avoid the pressure disturbance due to compressive storage and adsoprtion/desorption effect during the course of measurement. Hannon [17] provided a bidirectional model of pressure-pulse decay permeametry, which reaches equilibrium more than 7.5 times faster than the standard pressure-pulse decay. The pressure decay will

deviate from the exponential behavior in the early-time period, and considerable error may result if early-time data are used for permeability calculation [18, 19]. As a result, most of the authors [12, 15, 19–21] used the late-time measurements for permeability calculation. On the other hand, the early-time measurements may contain important information about the rock samples. For example, Kamath et al. [22] employed early-time data to estimate heterogeneity in the sample and Zhao et al. [23] utilized early-time data to analyze the nonlinear flow behavior. However, the time point differentiating the early-time and late-time behavior was not clearly defined and was often somewhat arbitrary in literature. The objective of this study is to develop a physically sound and mathematically accurate method for differentiating the early-time and late-time behavior.

2. Method for Differentiating the Early-Time and Late-Time Behavior

2.1. Early-Time and Late-Time Behavior. The governing equation for fluid flow in the core sample using the pressure-pulse decay method can be specified as follows [9, 11]:

$$\frac{\partial p^2(x,t)}{\partial x^2} = \frac{c\mu\phi}{k}\frac{\partial p(x,t)}{\partial t}, \tag{1}$$

with initial and boundary conditions:

$$\begin{aligned} &p(x,0) = p_2(0) \quad \text{for } 0 < x < L,\\ &p(0,t) = p_1(t) \quad \text{for } t \geq 0,\\ &p(L,t) = p_2(t) \quad \text{for } t \geq 0,\\ &\frac{dp_1}{dt} = \frac{k}{c\mu\phi L}\frac{V_S}{V_u}\frac{\partial p}{\partial x}\Big|_{x=0} \quad \text{for } t > 0,\\ &\frac{dp_2}{dt} = -\frac{k}{c\mu\phi L}\frac{V_S}{V_d}\frac{\partial p}{\partial x}\Big|_{x=L} \quad \text{for } t > 0, \end{aligned} \tag{2}$$

where x denotes the distance along the sample; t is real time; L refers to sample length; c, μ, ϕ, and k refer to fluid compressibility, fluid viscosity, porosity, and permeability, respectively; V_s, V_u, and V_d refer to the volume of sample pore, upstream chamber, and downstream chamber, respectively; and p_1 and p_2 are the pressure of the upstream chamber and downstream chamber, respectively.

Brace et al. [9] assumed that the pressure gradient was constant along the length of the sample (i.e., $(\partial p^2(x,t))/\partial x^2 = 0$) and presented a simplified solution as

$$p_1 - p_f = \Delta p \frac{V_d}{V_u + V_d} e^{-\alpha t}, \tag{3}$$

in which

$$\alpha = \frac{kA}{\mu\beta L}\left(\frac{1}{V_u} + \frac{1}{V_d}\right), \tag{4}$$

where p_f is the final pressure when $t \to \infty$.

The general analytical solution of equation (1) in terms of dimensionless differential pressure,

$$\Delta p_D = \frac{p_1(t) - p_2(t)}{p_1(0) - p_2(0)}, \tag{5}$$

was presented by Dicker and Smits [11]:

$$\begin{aligned} \Delta p_D &= 2\sum_{m=1}^{\infty} S_m\\ &= 2\sum_{m=1}^{\infty} \exp\left(-t_D\theta_m^2\right)\\ &\quad \cdot \frac{a\left(b^2+\theta_m^2\right) - (-1)^m b\left[\left(a^2+\theta_m^2\right)\left(b^2+\theta_m^2\right)\right]^{0.5}}{\theta_m^4 + \theta_m^2\left(a + a^2 + b + b^2\right) + ab(a + b + ab)}, \end{aligned} \tag{6}$$

where θ_m are the roots of equation (7); a and b are the ratios of pore volume to upstream and downstream, respectively; and t_D is dimensionless time, defined in equation (8):

$$\tan\theta = \frac{(a+b)\theta}{\theta^2 - ab}, \tag{7}$$

$$t_D = \frac{kt}{c\mu\phi L^2}. \tag{8}$$

The analytical solution of equation (6) includes an early-time behavior and a late-time behavior. In the early-time period, the effect of the downstream boundary condition is not felt. Although the early-time data can be used to investigate heterogeneity in core samples [22], more information than can be obtained from flow tests along is required. Therefore, the late-time solution, dominated by the first term in equation (6), is recommended for routine permeability calculation [12, 19].

Jones [12] simplified equation (6) into a similar form as Brace et al.'s by introducing a factor "f" as

$$f = \frac{\theta^2}{a+b}. \tag{9}$$

Therefore, the late-time solution for predicting permeability was then given as

$$\alpha = \frac{fkA}{\mu\beta L}\left(\frac{1}{V_u} + \frac{1}{V_d}\right). \tag{10}$$

Brace's solution of equation (4) can be treated as a particular late-time solution of Dicker and Smits's for $f = 1$.

Dicker and Smits [11] present convincing reasons that the volume of upstream and downstream chambers should be equal. On one hand, equal volumes could keep the mean pore pressure constant. A desirable situation of symmetry can be created by making upstream and downstream volumes identical, which indicates that any pressure decreases in the upstream chamber can be offset by an equal downstream pressure increase. On the other hand, equal chamber

volumes make equation (6) become a single exponential quickly, since all even terms of equation (6) cancel when $a = b$. Figure 1 presents the relationship between dimensionless pressure and time obtained from the general analytical solution (equation (6)) for $a = b$. The dashed lines and the solid lines refer to the first term S_1 and all terms in the summation (equation (6)), respectively. The first term (i.e., the late-time solution), representing the single-exponential behavior of pulse decay curve, overlaps the general solution for almost the entire portion of pressure decay when a is small. However, with the increase of volume ratios a, the contributions of higher terms to the first term increase, leading to significant deviation of pressure decay curve from single-exponential behavior at the early time. Consequently, Jones [12] and Feng [19] recommend that the late-time pressure decay should be used for permeability calculation. However, neither of them figured out the time point differentiating the early-time and late-time behavior.

2.2. Contribution Rate and Critical Time. Figure 2 shows the first six terms of the series in equation (6). As can be seen from the figure, the first term dominates and the remaining terms vanish after a certain time. Therefore, a contribution rate η is defined as the contribution of the first term to all terms in equation (6), which can be expressed as

$$\eta = \frac{S_1}{\sum_{m=1}^{\infty} S_m}, \tag{11}$$

where S_m is the mth term in equation (6). As the contribution ratio η approaches to 1 (i.e., the first term overlaps the general solution), the early-time behavior can be neglected. At this time, a time point can be obtained from equation (11) when η is estimated. We define such time point, t_c, as "critical time." Note that the accuracy of estimating η will significantly influence the critical time t_c.

Figure 3 shows the evolution of critical time t_c with η. Two distinct features can be seen from Figure 3. First, it is apparent that an increasing trend of critical time t_c can be observed when η increases. This is an indication that the period of early-time prolongs and more early-time data should be discarded when calculating permeability. Second, the critical time first increases when the volume ratio a is lower than a certain value (about 1, i.e., the pore volume equals to the chamber volume) and then decreases when the volume ratio is higher than that value.

The accuracy in permeability measurement mainly depends on the slope of late-time solution. To investigate the influence of contribution ratio η on permeability calculation, the slope of late-time solution was calculated under variable η values. Table 1 shows the analytical results of the slope and error coefficient at varied η values. Note that the slope at an η value of 99.999% was taken as a reference. It can be seen that the error coefficient is completely negligible when volume ratios are small. However, the influence of contribution ratio η on the permeability calculation becomes strengthened when $a > 1$ (e.g., small volume chambers are used). Specifically, when $a = b = 10$, the error coefficient (χ) increases from 0.041% to 10.645% with contribution ratio η ranging from

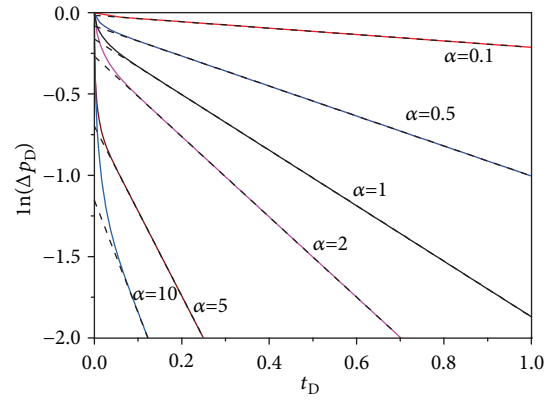

Figure 1: A comparison of the general solution (equation (6), the solid curves) with the first term of equation (6) (the dashed curves) for different ratios of pore volume to chamber volume (assuming the volume of upstream chamber equals to that of the downstream chamber, i.e., $a = b$).

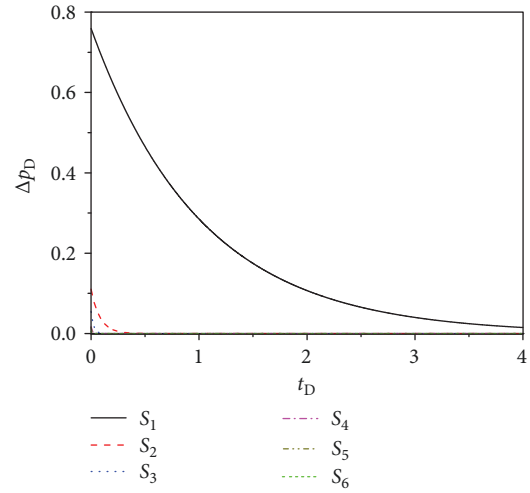

Figure 2: The first six terms of the series in equation (6) ($a = 1$ and $b = 0.2$).

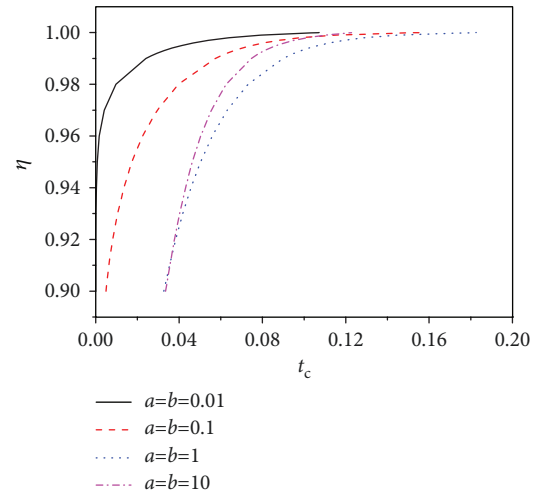

Figure 3: The evolution of critical time t_c with η in cases with same chamber sizes.

Table 1: Error coefficient χ at varied η values.

Volume ratios	90%		95%		99%		99.9%		99.99%	
	Slope	χ (%)	Slope	χ (%)	Slope	χ (%)	Slope	χ (%)	Slope	χ (%)
$a = b = 0.01$	0.020	0	0.020	0	0.020	0	0.020	0	0.020	0
$a = b = 0.1$	0.197	0	0.1967	0	0.1967	0	0.197	0	0.197	0
$a = b = 1$	1.710	0.185	1.709	0.089	1.707	0.021	1.707	0.001	1.707	0.001
$a = b = 10$	7.672	10.645	7.361	6.165	7.055	1.745	6.950	0.228	6.937	0.041

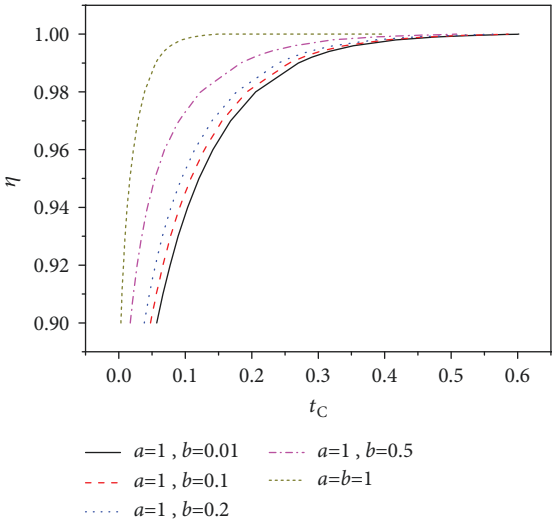

Figure 4: Critical time of cases with unequal chamber sizes.

90% to 99.99%. This will lead to at least 10.645% of the computation error of permeability. Therefore, a high η value (>99.9%) is recommended when small volume chambers are used.

2.3. The Influence of Unequal Chamber Sizes on Critical Time. Different chamber sizes between upstream and downstream have been chosen by some scholars to have a speed-up of the measurement [24, 25]. However, such configuration increases the period of early time significantly. As shown in Figure 4, the critical time for cases with same chamber size is less than 0.2, but it increases to about 0.4 for cases with unequal chamber size due to the contribution of even terms in equation (6). Meanwhile, as the ratio of a to b increases, the critical time increases at a certain η value.

2.4. Physical Sound of Late Time. A numerical simulator, TOUGH+REALGASBRINE (TOUGH+), is employed to simulate pressure-pulse decay tests. TOUGH+ is based on a finite volume approach and is a successor to the TOUGH2 family of codes for fluid and heat flow [26]. In the numerical tests, the chambers and core sample are assumed as parts of one system. To simulate an actual chamber, the porosity of the chamber is set to 1, and large permeability values are used. 102 column elements (2 for chambers, 100 for rock sample) are built in the numerical model. Since the dimensionless differential pressure mainly depends on volume ratios, four cases involving different volume ratios in magnitude order are numerically calculated. The operating parameters are listed in Table 2.

Figure 5 shows the pressure gradient along sample length over time elapsed. As can be seen from the figures, the pressure gradient along the sample varies nonlinearly at the early time. After the time over t_c, a constant pressure gradient is attained, which not only illustrates that the early time cannot be applied for permeability calculation but also illuminates the usefulness of our method for determination of critical time. Moreover, when a is small, the early-time period is in seconds (real time) and the pressure gradient is constant over most of its range (Figure 4(a)). When a is large, the early-time period could be minutes or even hours, and the pressure gradient becomes constant only at the late time. This suggests that the most important assumption of Brace's solution, assuming a constant pressure gradient, is invalid when a is small.

3. Application to Permeability Measurement

In this section, we applied the method of differentiating the early-time and late-time behavior into laboratory permeability tests. Previous studies [12, 16] demonstrated that a smaller volume chamber could trigger faster pressure-pulse decay and thus reduce the measurement time. The price to be paid for the time saving is that more early time must be discarded during the process of permeability calculation. To experimentally investigate the effect of volume ratio on the permeability measurement, two sets of experiments with different volume ratios are carried out on a self-made "Triaxial Seepage System for Rock (TSSR)" (Figure 6). The detailed experimental schemes are listed in Table 3.

3.1. Equipment. TSSR system is composed of five main units: triaxial cell, loading unit, temperature control unit, vacuum unit, and data collection unit. The experimental setup (shown in Figure 6) is mainly configured with a transient flow apparatus for the permeability test of rocks and is capable of measuring rock permeability under different stress fields, pore pressures, and temperatures. The system can also allow the calculation of the pore volume from Boyle's law. Confining pressure and axial stress are loaded to the core sample by a hydraulic water pump. Gas pressure is controlled by cooperation of a pressurized gas pumping system and a pressure reducing valve. Prior to gas flow tests, the chamber volumes are calibrated using an impermeable stainless-steel

Table 2: Modeling parameters of numerical tests.

Parameters	Case 1 ($a = b = 0.01$)	Case 2 ($a = b = 0.1$)	Case 3 ($a = b = 1$)	Case 4 ($a = b = 10$)
Chamber volume (cm^3)	196	19.6	19.6	1.96
Core length (m)	0.1	0.1	0.1	0.1
Core diameter (m)	0.05	0.05	0.05	0.05
Pore pressure (MPa)	1	1	1	1
Pulse pressure (MPa)	0.1	0.1	0.1	0.1
Porosity	0.01	0.01	0.1	0.1

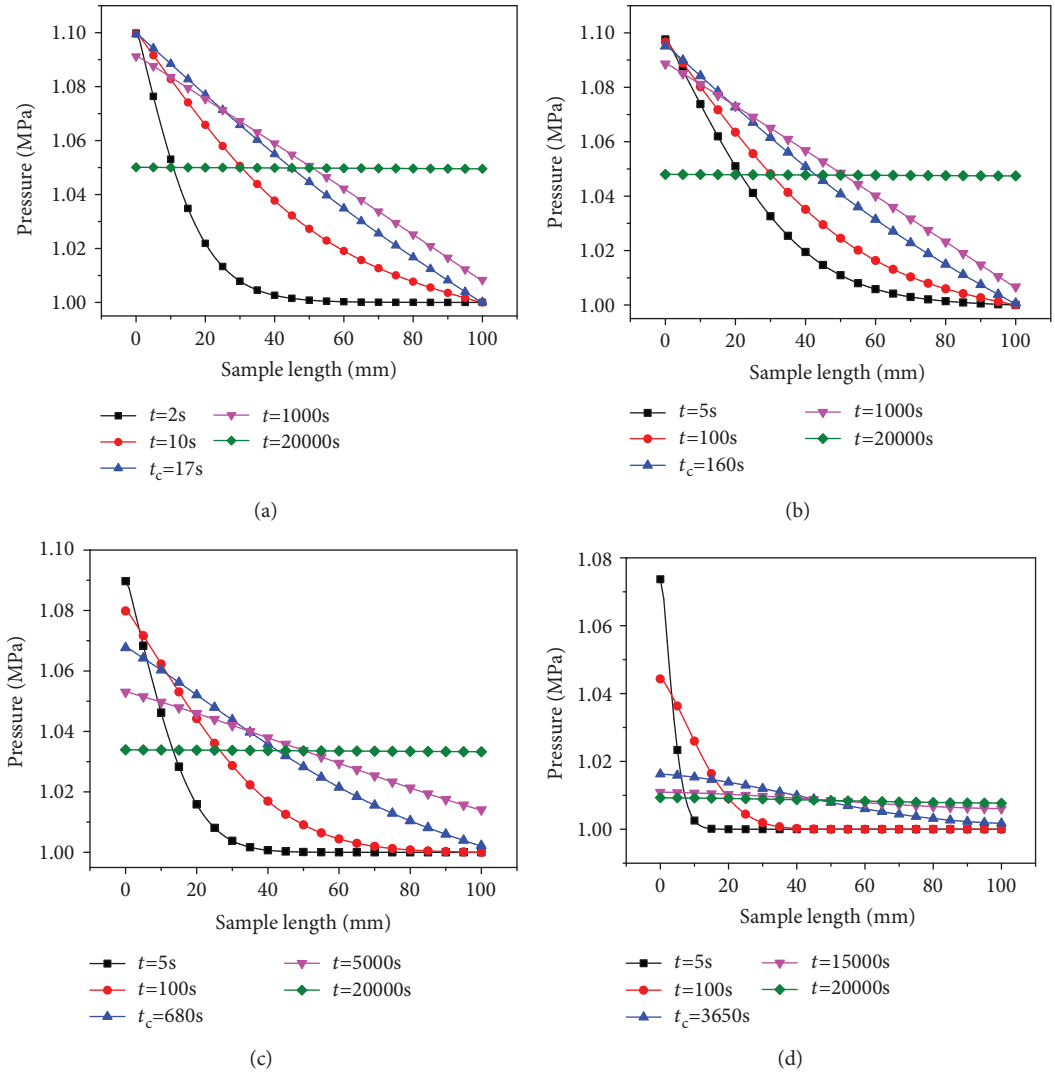

Figure 5: Pressure responses along the length of the sample at different real times: (a) case 1, (b) case 2, (c) case 3, and (d) case 4.

sample, yielding the upstream and downstream volumes of 23.6 cm^3 and 20.0 cm^3, respectively.

3.2. Sample Preparation. Shale and rock-like sample, with significant difference in pore volume, were selected for experimental study. The rock-like sample, with dimensions of 50 mm in diameter and 100 mm in length, was made of a mixture of ordinary Portland cement, sand, and water at a ratio of 1 : 1.2 : 0.65 [27].

Blocks of shale sample were first extracted from a quarry located in Liutang in Shizhu Country, China. Then, a cylindrical core sample with dimensions of 50 mm in diameter was sampled from the shale block. The length of the shale sample was cut to 33.5 mm for two purposes. For one thing,

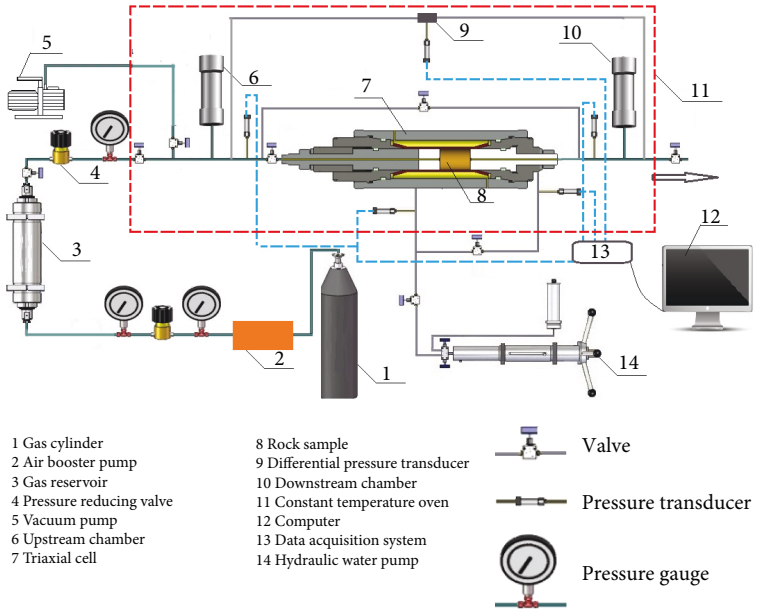

Figure 6: Experimental setup for pulse-decay permeability measurements. 1: gas cylinder; 2: air booster pump; 3: gas reservoir; 4: pressure reducing valve; 5: vacuum pump; 6: upstream chamber; 7: triaxial cell; 8: rock sample; 9: differential pressure transducer; 10: downstream chamber; 11: constant temperature oven; 12: computer; 13: data acquisition system; 14: hydraulic water pump.

Table 3: Experimental schemes of test 1 and test 2.

		Test 1	Test 2
Rock type		Shale	Rock-like material
Sample size		$\phi 50 \times 33.5$ mm	$\phi 50 \times 100$ mm
Testing condition		Constant effective stress	Varied effective stress
Volume ratio	a	0.059	1.32~1.60
	b	0.069	1.55~1.88

the shorter the length is, the smaller the pore volume will be. For another, a short length helps to reduce measurement time since shale has ultralow permeability. The density of the shale sample is 2.55 g/cm^3, and the porosity is 2.0%. Figures 7 and 8 show the well-prepared samples and their pore characteristics. It can be seen that the pore diameter of shale (less than 1 μm) is much smaller than that of the rock-like sample (about 1.8 mm).

3.3. Experimental Procedures. The permeability tests were carried out using the conventional pressure-pulse decay proposed by Brace et al. [9]. The pure gas used in this study was He at a purity of 99.999%. The system was kept to be initially at a uniform pore pressure throughout. Then, the pressure of upstream was increased suddenly to produce a pressure difference. The pressure-time responses were recorded to estimate permeability. Test 1 was conducted at constant effective stress of 3 MPa to keep the pore volume unchanged. While test 2 was conducted at a constant pore pressure of 2 MPa and confining pressures ranging from 5 MPa to 20 MPa to investigate the effects of pore volume on pressure decay. Note that all these tests were conducted at high pore pressure (≥2 MPa) to reduce the effects of gas slippages.

3.4. Experimental Results. When the dimensionless differential pressure is plotted with dimensionless time, the curves of test 1 will be similar and situated close to each other due to the constant pore volume. Examination of Figure 9(a) shows that this is indeed the case. Another feature which can be observed in Figure 9(a) is that almost all pressure data follow the exponential behavior. This illustrates that as the volume ratio takes on small values, the role played by the early-time pressure response in permeability estimation is negligible; therefore, no additional work is needed to differentiate the early-time and late-time behavior. Moreover, to demonstrate the validity of the tests, the exact analytical solution (equation (6)) is also plotted in Figure 9(a). The figure clearly illustrates that the experimental results and analytical results matched each other very well, supporting the success of our tests.

Figure 9(b) shows the experimental results of test 2. In the semilogarithmic graph, the early-time behavior deviates from a straight line significantly due to the contribution of higher terms; thus, considerable errors in permeability may result if the early-time data is used. From Figure 9(b), we also see that the slope of the straight line part decreases with the confining pressure due to the reduction of pore volume, which comes with a weaker deviation. This indicates that the contribution of higher terms decreases with pore volume reduction. Then, the critical time is calculated through equation (11). The late-time data were fitted by a linear function as plotted in Figure 9(b). The permeability of the core sample, therefore, can be computed from the slope of the late-time fitting lines by equation (10). Table 4 shows the estimated

(a) (b) (c)

Figure 7: Rock-like sample: (a) vertical section, (b) cross section, and (c) image from CT scanning.

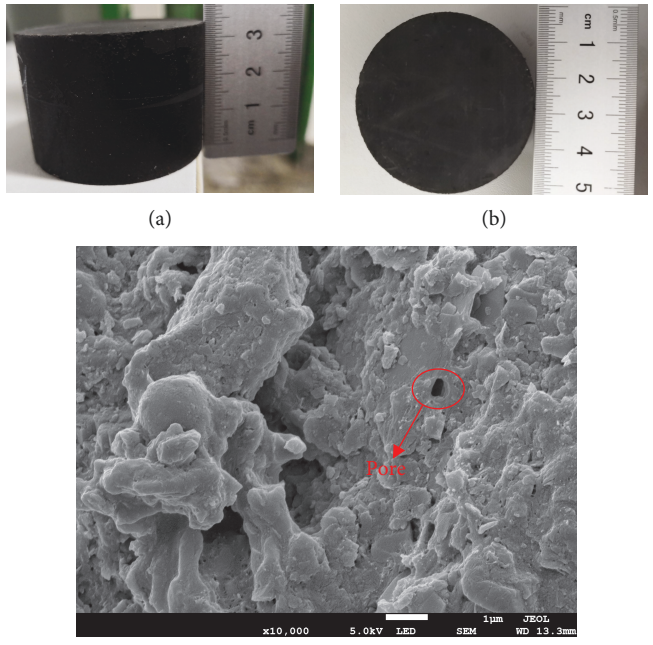

(a) (b)

(c)

Figure 8: Shale sample: (a) vertical section, (b) cross section, and (c) image from SEM scanning.

permeability of samples using the late-time pressure data. As expected, the permeability decreases with the increase of confining pressure.

4. Conclusion

The early-time pressure decay data cannot be used for permeability estimation in pressure-pulse tests though it is useful for sample heterogeneity investigation. A method for differentiating the early-time and late-time behavior is proposed. It is validated by a TOUGH+ simulator and is applied into the laboratory tests for permeability calculation. Based on the work completed, the conclusions are summarized as follows:

(1) As the volume ratio increases, the critical time appears to have a declining trend after an initial ascent. The critical time for cases with same chamber volumes is much less than that for cases with unequal chamber volumes

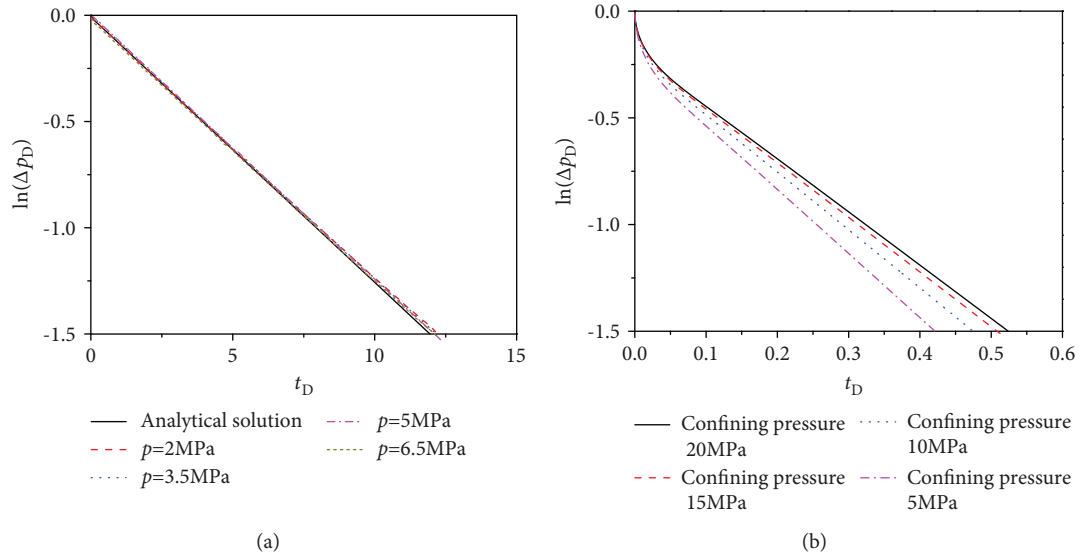

Figure 9: The relationship of dimensionless pressure and time: (a) shale sample and (b) rock-like sample.

Table 4: Experimental schemes and permeability results of test 1 and test 2.

	Sample	Size (mm)	Confining pressure (MPa)	Pore pressure (MPa)	Permeability (m^2)
Test 1	Shale sample	$\phi 50 \times 33.5$	5	2	1.59×10^{-18}
			6.5	3.5	1.49×10^{-18}
			8	5	1.45×10^{-18}
			9.5	6.5	1.44×10^{-18}
Test 2	Rock-like sample	$\phi 50 \times 100$	5	2	7.37×10^{-17}
			10	2	4.53×10^{-17}
			15	2	3.06×10^{-17}
			20	2	2.31×10^{-17}

(2) The numerical results show that the pressure gradient along the sample varies nonlinearly at the early time and becomes a constant at the late time. The time for pressure gradient to attain constant increases with volume ratios; it could be hours for pressure gradient to attain constant at large volume ratios

(3) The early-time behavior is negligible when the volume ratio is smaller than 0.1. With the increase of volume ratios, the deviation of pulse decay curve from single-exponential behavior increases, and the late-time data should be used for permeability calculation

Data Availability

All the data and computer codes for this paper can be available by contacting the corresponding author, whose email address is as follows: zytyut1@126.com. They can also be obtained by contacting the first author, whose email address is as follows: 20151601005@cqu.edu.cn.

Conflicts of Interest

The authors declare that they have no conflicts of interest.

Acknowledgments

This research was supported by the National Natural Science Foundation of China (No. 51374257 and No. 50804060). It was also supported by the China Scholarship Council (CSC) for the second author's visit at the Lawrence Berkeley National Laboratory. The authors would like to acknowledge Lehua Pan from the Lawrence Berkeley National Laboratory for the continuous encouragement and guidance.

References

[1] R. Sander, Z. Pan, and L. D. Connell, "Laboratory measurement of low permeability unconventional gas reservoir rocks: a review of experimental methods," *Journal of Natural Gas Science and Engineering*, vol. 37, pp. 248–279, 2017.

[2] S. Salahshoor, M. Fahes, and C. Teodoriu, "A review on the effect of confinement on phase behavior in tight formations," *Journal of Natural Gas Science and Engineering*, vol. 51, pp. 89–103, 2018.

[3] Z. J. Pan, J. P. Ye, F. B. Zhou, Y. Tan, L. D. Connell, and J. Fan, "CO2 storage in coal to enhance coalbed methane recovery: a review of field experiments in China," *International Geology Review*, vol. 60, pp. 754–776, 2018.

[4] J. Rutqvist, D. W. Vasco, and L. Myer, "Coupled reservoir-geomechanical analysis of CO2 injection and ground deformations at In Salah, Algeria," *International Journal of Greenhouse Gas Control*, vol. 4, pp. 225–230, 2010.

[5] R. Senger, E. Romero, and P. Marschall, "Modeling of gas migration through low-permeability clay rock using information on pressure and deformation from fast air injection tests," *Transport in Porous Media*, vol. 123, no. 3, pp. 563–579, 2018.

[6] S. M. Hassanizadeh, M. A. Celia, and H. K. Dahle, "Dynamic effect in the capillary pressure-saturation relationship and its impacts on unsaturated flow," *Vadose Zone Journal*, vol. 1, no. 1, pp. 38–57, 2002.

[7] B. Ataie-Ashtiani, S. Majid Hassanizadeh, and M. A. Celia, "Effects of heterogeneities on capillary pressure-saturation-relative permeability relationships," *Journal of Contaminant Hydrology*, vol. 56, no. 3-4, pp. 175–192, 2002.

[8] L. Zhuang, S. M. Hassanizadeh, C. Z. Qin, and A. de Waal, "Experimental investigation of hysteretic dynamic capillarity effect in unsaturated flow," *Water Resources Research*, vol. 53, pp. 9078–9088, 2017.

[9] W. F. Brace, J. B. Walsh, and W. T. Frangos, "Permeability of granite under high pressure," *Journal of Geophysical Research*, vol. 73, pp. 2225–2236, 1968.

[10] P. Hsieh, J. Tracy, C. Neuzil, J. Bredehoeft, and S. Silliman, "A transient laboratory method for determining the hydraulic properties of 'tight' rocksdI. Theory," *International Journal of Rock Mechanics and Mining Science and Geomechanics Abstracts*, vol. 18, pp. 245–252, 1981.

[11] A. Dicker and R. Smits, "A practical approach for determining permeability from laboratory pressure-pulse decay measurements," in *International Meeting on Petroleum Engineering*, Tianjing, China, 1988.

[12] S. C. Jones, "A technique for faster pulse-decay permeability measurements in tight rocks," *SPE Formation Evaluation*, vol. 12, pp. 19–26, 1997.

[13] X. Cui, A. M. M. Bustin, and R. M. Bustin, "Measurements of gas permeability and diffusivity of tight reservoir rocks: different approaches and their applications," *Geofluids*, vol. 9, 223 pages, 2009.

[14] D. Lasseux, Y. Jannot, S. Profice, M. Mallet, and G. Hamon, *The 'Step Decay': a New Transient Method for the Simultaneous Determination of Intrinsic Permeability, Klinkenberg Coefficient and Porosity on Very Tight Rocks*, Presented at the International Symposium of the Society of Core Analysts, Aberdeen, Scotland, 2012.

[15] Z. Yang, Q. Sang, M. Dong, S. Zhang, Y. Li, and H. Gong, "A modified pressure-pulse decay method for determining permeabilities of tight reservoir cores," *Journal of Natural Gas Science and Engineering*, vol. 27, pp. 236–246, 2015.

[16] R. Feng, J. Liu, and S. Harpalani, "Optimized pressure pulse-decay method for laboratory estimation of gas permeability of sorptive reservoirs: part 1-background and numerical analysis," *Fuel*, vol. 191, pp. 555–564, 2017.

[17] M. J. Hannon, "Alternative approaches for transient-flow laboratory-scale permeametry," *Transport in Porous Media*, vol. 114, no. 3, pp. 719–746, 2016.

[18] J. He and K. Ling, "Measuring permeabilities of Middle-Bakken samples using three different methods," *Journal of Natural Gas Science and Engineering*, vol. 31, pp. 28–38, 2016.

[19] R. Feng, "An optimized transient technique and flow modeling for laboratory permeability measurements of unconventional gas reservoirs with tight structure," *Journal of Natural Gas Science and Engineering*, vol. 46, pp. 603–614, 2017.

[20] T. Chen and P. W. Stagg, "Semilog analysis of the pulse-decay technique of permeability measurement," *Society of Petroleum Engineers. Journal*, vol. 24, pp. 639–642, 1984.

[21] H. Darabi, A. Ettehad, F. Javadpour, and K. Sepehrnoori, "Gas flow in ultra-tight shale strata," *Journal of Fluid Mechanics*, vol. 710, pp. 641–658, 2012.

[22] J. Kamath, R. Boyer, and F. Nakagawa, "Characterization of core scale heterogeneities using laboratory pressure transients," *SPE Formation Evaluation*, vol. 7, pp. 219–227, 1992.

[23] Y. L. Zhao, L. Y. Zhang, W. J. Wang, J. Z. Tang, H. Lin, and W. Wan, "Transient pulse test and morphological analysis of single rock fractures," *International Journal of Rock Mechanics and Mining Sciences*, vol. 91, pp. 139–154, 2017.

[24] H. J. Sutherland and S. P. Cave, "Argon gas permeability of New Mexico rock salt under hydrostatic compression," *International Journal of Rock Mechanics and Mining Science and Geomechanics Abstracts*, vol. 17, no. 5, pp. 281–288, 1980.

[25] Y. M. Metwally and C. H. Sondergeld, "Measuring low permeabilities of gas-sands and shales using a pressure transmission technique," *International Journal of Rock Mechanics and Mining Sciences*, vol. 48, no. 7, pp. 1135–1144, 2011.

[26] G. J. Moridis and K. Pruess, *User's Manual of the TOUGH+ Core Code v1.5: a General-Purpose Simulator of Non-Isothermal Flow and Transport through Porous and Fractured Media, Report LBNL-1871E*, Lawrence Berkeley National Laboratory, Berkeley, CA, 2014.

[27] Y. L. Zhao, L. Y. Zhang, W. J. Wang, C. Z. Pu, W. Wan, and J. Z. Tang, "Cracking and stress-strain behavior of rock-like material containing two flaws under uniaxial compression," *Rock Mechanics and Rock Engineering*, vol. 49, pp. 2665–2687, 2016.